Soil & Tillage Research 248 (2025) 106468

Contents lists available at ScienceDirect

Soil & Tillage Research

journal homepage: www.elsevier.com/locate/still

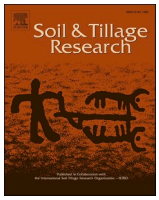

Air-filled porosity, its connectivity and relation to particulate organic matter in intact soil cores controls carbon emissions near saturation

Elsa Coucheney [a,*,1], Emilien Casali [a], Nicholas Jarvis [a,2], Johannes Koestel [a,b,3]

[a] Department of Soil and Environment, Swedish University of Agricultural Sciences, Lennart Hjelms väg 9, Uppsala 756 51, Sweden
[b] Department of Agroecology and Environment, Reckenholzstrasse 191, Zürich 8046, Switzerland

ARTICLE INFO

Keywords:
Carbon emissions
Intact soil cores
X-ray tomography
Air-filled porosity
No-till
Wet soil conditions

ABSTRACT

In wet soils, oxygen (O_2) transport in large structural pores that drain close to saturation limits SOC mineralization and C emissions. However, these effects are still poorly understood because in standard incubation experiments soils are sieved and structural pore networks are destroyed. Our objective was to investigate the effects of soil structure on C mineralization rates under wet soil conditions. We measured CO_2 emissions from intact soil cores of contrasting structure taken from conventional tillage vs. no-till treatments in laboratory incubations at pressure heads ranging from saturation to −30 cm. At each drainage step, we used X-ray CT to quantify various metrics of the geometry and topology of air, soil matrix and particulate organic matter (POM). We show that CO_2 emissions are regulated by the air-filled porosity connected to the soil surface, as well as by the area of the interface between this connected air phase and the soil matrix and the volume of the matrix located within 2–3 millimetres of the interface and POM in this "active" zone. All four of these variables increase concomitantly with air-entry, although in the case of no-till soils, CO_2 emissions increased most rapidly during initial drainage. We attributed this to the more heterogeneous "space-filling" pore structure and a larger fraction of bio-pores found in the no-till cores. These results should help to support the development of improved models of SOC turnover taking into account the effect of soil structure and soil management.

1. Introduction

Soils and climate are interconnected systems and the result of their complex interactions together with vegetation and land management is critically important for the carbon balance in the soil-plant-atmosphere system (Certini and Scalenghe, 2023). Changes in soil organic matter stocks and the release of C back into the atmosphere affect both soil quality (Stockmann et al., 2015) and climate regulation (Jungkunst et al., 2022). Indeed, soil organic matter is recognized as one of the most important factors sustaining soil quality through, for example, its effects on the soil biological habitat and soil fertility (Franzluebbers, 2002; Krause et al., 2022; Reeves, 1997) as well as on soil physical conditions (Lal, 2013; Henryson et al., 2018; Meurer et al., 2020). For these reasons, a sound understanding of the controls on organic matter mineralization rates in soil is therefore of critical importance for both soil quality itself and the feedbacks to climate via the release of CO_2.

Climate affects the soil temperature and moisture regimes that directly regulate organic matter decomposition (Sierra et al., 2015; Rey et al., 2005; Curiel Yuste et al., 2007). Soil moisture has been identified as one of the most sensitive components determining the effects of climate change on SOM turnover (Garten et al., 2009). However, the *in situ* relationship between C emissions and variations in soil moisture is complex due to many interactions with other factors (Hursh et al., 2017, Wickland and Neff, 2008, González-Domínguez et al., 2019). For example, climate controls soil moisture via diverse interactions with soil-plant system properties (Feng et al., 2023), while soil moisture and soil properties regulate soil geochemical processes and organic carbon dynamics interactively (Doetterl et al., 2015).

Controlled soil incubation experiments have therefore been used to support the derivation of theoretical and empirical functions describing

* Corresponding author.
E-mail addresses: elsa.coucheney@slu.se (E. Coucheney), emilien.casali@outlook.fr (E. Casali), nicholas.jarvis@slu.se (N. Jarvis), johannes.koestel@agroscope.admin.ch (J. Koestel).
[1] 0000–0001-5988–2085
[2] 0000–0001-6725–6762
[3] 0000–0002-3230–5699

https://doi.org/10.1016/j.still.2025.106468
Received 15 July 2024; Received in revised form 20 December 2024; Accepted 18 January 2025
Available online 26 January 2025

the response of C mineralisation to soil moisture (Moyano et al., 2012; Sierra et al., 2015) that are widely used in soil organic matter turnover models (e.g. Braakhekke et al., 2011, Linkosalo et al., 2013). In turn, these models are also embedded within broader modelling platforms describing water, nutrient and organic matter cycling in the soil-plant-atmosphere system (e.g. Gabrielle et al., 2002; Yin et al., 2020). However, the inclusion of climatic regulation via soil moisture inside Earth System Models used for climate predictions is still a matter of discussion and underrepresented. This is because the response of C mineralization to variations in soil moisture is still not well understood (Evans et al., 2022; Pallandt et al., 2022; Sierra et al., 2015). Indeed, the effects of soil moisture on C mineralization rates are the outcome of complex interactions between both biological (e.g. the activity of microbial communities) and physical (e.g. diffusion rates of substrate and oxygen) processes which take place in a complex porous medium that is highly structured at multiple scales (Baveye et al., 2018). For example, the composition and spatial distribution of both organic matter and microbial communities is heterogeneous both between and within different classes of pore size (Kuzyakov and Blagodatskaya, 2015, Chakrawal et al., 2020; Nunan et al., 2003; Rawlins et al., 2016, Chatterjee et al., 2024). Moreover, soil structure is known to exert a significant control on the distributions of water and air in soil and thus the diffusion rates of O_2 and solutes (e.g. substrate) and in turn their accessibility to decomposition by microbial communities (Peth et al., 2014). In soils of undisturbed structure, active microbial populations and hotspots for C turnover (e.g. Heitkötter and Marschner, 2018a,b) are often confined to the connected networks of macropores (e.g. biopores and aggregate surfaces; Yoo et al., 2006; Kuzyakov and Blagodatskaya, 2015; Leue et al., 2018; 2021; Liang et al., 2021) that quickly drain after rain events. Intensive tillage homogenizes soil pore size distributions (Kravchenko et al., 2011; Wang et al., 2012) and organic carbon concentrations (e.g. Ananyeva et al., 2013) and also affects microbial biomass and activity (Sun et al., 2020; Zhang et al., 2023). Yet most incubation experiments that have investigated the regulation of CO_2 emissions by soil moisture have been carried out on sieved soil in which the undisturbed structure of the soil '*in situ*' has been destroyed. The relevance of these findings for soils of intact structure under field conditions is therefore questionable, especially for systems with reduced tillage or no-till management (Herbst et al., 2016).

Imaging techniques afford the possibility to quantify relationships between the structure and functions of undisturbed soils (Helliwell et al., 2013; Schlüter et al., 2014). X-ray CT in particular is well suited to studying relationships between soil pore space structure and C emissions from soil (e.g. Kravchenko and Guber, 2017). In this respect, recent studies have demonstrated the important role of physical protection (i.e. inaccessibility to microbial decomposition) in regulating the decomposition rates of particulate organic matter (Toosi et al., 2017; Quigley et al., 2018). Other studies have used X-ray to investigate the long-term effects of tillage systems and land use on soil pore structure and CO_2 emissions (e.g. Alskaf et al., 2021; Ghosh et al., 2022). Little attention so far has been focused on using imaging techniques to specifically study the role of soil moisture in mediating the effects of soil structure on mineralization. Li et al. (2022) used X-ray to study the effects of soil moisture on mineralization of particulate organic matter in incubations carried out under optimal and dry soil conditions. Schlüter et al. (2022) measured carbon mineralization in soil aggregates from three grassland and agricultural soils and showed that mineral-associated organic matter was depleted around pores with diameters larger than 10 μm under both partially and fully saturated conditions. Recently, Lucas et al. (2024) investigated the effects of the distribution of particulate organic matter (POM) in intact soil cores on soil respiration and denitrification and showed the importance of the distance of POM to air-filled pores in explaining CO_2 emissions. To the best of our knowledge, this is the only study that has used X-ray CT to investigate CO_2 emissions in intact soils close to saturation where O_2 limitation is expected to regulate C mineralization. Furthermore, no previous studies have used X-ray CT to investigate the long-term effects of contrasting tillage systems on the soil structural pore space and how these differences in soil structure influence CO_2 emissions close to saturation. These are important knowledge gaps as wet soil conditions commonly occur, for example in irrigated agriculture (e.g. paddy rice fields) or during autumn and winter in temperate climates where agricultural soils can be left bare. Under such conditions, mineralization of organic matter (e.g. incorporated crop residues) may be significant, leading to risks of nutrient leaching. O_2 availability under wet soil conditions is also a highly relevant factor regulating the decomposition of C in subsoils (e.g. Salome et al., 2010), which usually contains a significant fraction of the total C stock in the soil profile (e.g. Rumpel and Kögel-Knabner, 2011). Wetter soil conditions may also occur more often in the future, at least in some regions, due to more frequent intense rain events and subsequent flooding in a warming climate (IPCC, 2021).

The objective of this study was therefore to investigate the relationships between C emissions close to saturation and the volume and connectivity of the air-filled porosity for intact soil cores taken from two contrasting tillage treatments (conventional tillage vs. no-till). We hypothesized that differences in C emissions close to saturation are to a large part due to the contrasting volumes and surface areas of connected air-filled porosity and their spatial relationships (distances) to sources of organic matter as they regulate O_2 availability for microbial activity through their role for diffusive gas transport in air and water and gas dissolution at the air/water interface. Additionally, we further expected that the relationships between C emissions and metrics quantifying the amount and distribution of soil air close to saturation would differ between cultivated and undisturbed soils because of contrasts in the soil pore network architecture as well as the number and type of soil macropores (e.g. biopores), as well as the distances of such macropores to particulate organic matter (POM). To test these hypotheses, we combined measurements of CO_2 emissions with a quantification of soil air content and POM and their relative distribution by X-ray CT as the samples were stepwise drained at pressure heads decreasing from zero to −30 cm.

2. Materials and methods

2.1. Soil sampling

Soil samples were taken in October 2019 from a long-term experiment on annual cropping systems located at the environmental research and observatory site SOERE ACBB in northern France (Estrées-Mons, INRAe, France, 49°52′44″N 3°00′27″E). The soil is an Orthic Luvisol (FAO classification) and the 0–30 cm horizon has a silt loam texture (19 % clay, 76 % silt and 5 % sand) and a pH of 7.6 (Boizard et al., 2013; Lamichhane et al., 2021). One of the fields that was sampled is managed under conventional tillage practice corresponding to mouldboard ploughing to 30 cm depth in autumn/winter followed by secondary cultivation to produce a seedbed ca. 3–9 cm in thickness, while the other is under shallow tillage using a compact disc cultivator working at an average depth of 6 cm (ranging from ca. 4–8 cm). Soil core samples were taken at a depth of 10–15 cm, which is both below the depth of shallow cultivation and also avoided the dense root system from the mustard cover crop sown at that time. Therefore, the field under shallow tillage will be referred to as a '*no-till*' treatment hereafter, in contrast with the conventional tillage treatment with mouldboard ploughing, which will be referred to as the '*Till*' treatment. A greater faunal activity (biopores and worm casts) in the *no-till* treatment was visible at the field site at the time of sampling. Eight replicate aluminium soil cores of height 5 cm and inner diameter of 6.5 cm were sampled in four experimental blocks of each field (2 cores per block). Cores with soil of intact structure were transported in a cooled box and stored at 4 °C in sealed plastic bags until further analyses.

2.2. Soil characteristics and sample preparation

The base of each soil core was covered with a cloth held by a rubber band. Soil cores were taken out of the cold room inside their plastic bag, weighed to later estimate the water content at the time of sampling and were then left to adjust to room temperature over a period of 24 hours. Each sample was first wetted from the base by placing it in a shallow water bath (with a water depth of ca. 0.2–0.5 cm) for 48 hours. The cores were subsequently drained at a pressure head of −100 cm using a suction device (pF laboratory station with suction plate module, EcoTech) for 48 hours. The drainage process was followed by weighing the samples and equilibrium was assumed to have been reached when the water loss was negligible. This was followed by a week of pre-incubation at 20℃ to allow soil microbial communities to adjust to changes in temperature and water contents inside the core. C mineralization was measured after 1, 3 and 7 days to identify the peak of mineralization rates due to these disturbances (data not shown). At the end of the drainage/incubation experiment (see next section), all of the soil was extracted from the core, mixed and subsequently dried at 105°C to determine the dry soil weight and bulk density of each individual soil core. An aliquot of the mixed soil was then used to determine the soil organic C and N contents as well as the particle size distribution (PSD) using a Laser Scattering Particle Size Distribution Analyzer LA-950 (Nimblad Svensson et al., 2022).

2.3. Soil incubations and C emission measurements

The soil cores were successively incubated at decreasing pressure heads starting at near-saturated conditions resulting from the cores being equilibrated in a 1 cm deep water bath. We then continued to pressure heads at the base of the core of −10, −20 and −30 cm (equivalent to −1 to −3 kPa). At each step, the cores were first equilibrated on the suction plate and then incubations were carried out for a period of 6 days at a constant temperature of 20℃. The soil cores were placed on small pedestals in 1 L air-tight glass jars (Le Parfait®) together with 20 ml of water at the bottom of the jar to keep the air humidity in the jar close to saturation and to avoid soil desiccation. We also included a 20 ml Sterilin® Scintillation plastic vial filled with 17 ml of 0.05 M KOH solution (Potassium hydroxide pellets for analysis, EMSURE®) to trap CO_2 emitted inside the jar during each period of measurement. The CO_2 in the KOH solution was measured every 1–3 days. The jars were placed inside an incubator (Heratherm™ Refrigerated Incubator) set to a constant temperature (20℃) and with constant ventilation, together with 3 jars without any soil as blanks (i.e. to measure CO_2 inside the jar that is not related to soil C mineralisation).

The vials (i.e. CO_2 traps) were taken out of the jars and the amount of CO_2 trapped during the period of measurement was analysed immediately by measuring the electrical conductivity of the KOH solution using an electrical conductometer (WTW - Portable conductivity meter ProfiLine Cond 3310). The amount of CO_2 emitted was estimated from the difference between the conductivity of the solution after a few days of incubation and the conductivity measured in solutions placed inside the blanks (containing only the initial KOH solution), as conductivity is proportional to the amount of CO_2 trapped in the solution (Chapman, 1971; Smirnova et al., 2014). Prior to the next measurement period, the jars were aerated and new KOH traps were placed in them. Carbon mineralization rates were measured three times during the incubation period, after 1, 3 and 6 days. The measurement made on day 1 was always higher than on days 3 and 6, presumably due to disturbance as a result of the change in soil moisture conditions and was therefore discarded. In contrast, the averages of the rates measured after 3 and 6 days were not significantly different overall and were regarded as the basal respiration rate in further analyses, representative of a quasi-steady-state under the prevailing moisture conditions. Carbon emission rates were expressed as μg C-CO_2 per g of soil organic C (instead of g soil) to remove the potential effects of variations in C content among the intact soil cores. However, C emission rates expressed per g of soil are presented in the supplementary material (Table S1).

After one day of incubation at each pressure head, half of the cores were scanned by X-ray (see next section) in order to quantify the X-ray visible air-filled porosity. The samples were kept outside the incubator for 5 hours each time, but the temperature in the X-ray laboratory was also set at 20 °C to minimize any perturbations due to changes in temperature. The remaining soil cores were kept in the incubator as controls to assess the potential effects of X-ray scanning on C emissions. No significant differences in C mineralization rates between the cores submitted to X-ray or kept inside the incubator were found, which is in agreement with the results of Bouckaert et al. (2013) and Schmidt et al. (2015).

2.4. X-ray scanning and image analysis

X-ray scanning and image analysis was carried out on eight intact cores (four from each tillage treatment) equilibrated at four different pressure heads at the base ($\Psi = 0$, −10, −20 and −30 cm). The images were acquired with a GE Phoenix v|tome|x240 industrial X-ray scanner equipped with a GE 16″ flat panel detector with 2014 × 2014 detector crystals (GE DRX250RT). We set the tube voltage at 140 kV with an electron flux of 350 μA and included 0.3 mm of copper foil into the beam trajectory to reduce beam-hardening artefacts. Each scan consisted of 2000 radiographs with an isometric voxel edge length of 43 μm. This resulted in an image resolution of approximately 100 μm, which corresponds to the largest diameter of water-filled pores at a pressure head of −30 cm following the Young-Laplace equation and assuming perfect wettability. Thus, the metrics of the air phase (see below) measured at the smallest pressure head in the incubation experiment should mostly reflect the pore network itself. The radiographs were inverted to 3-D images using the GE software datos|x (version 2.1).

Image analysis was carried out using ImageJ/FIJI (Schindelin et al., 2012) with the plugin SoilJ (Koestel, 2018). First, we filtered the images with a 2x2x2 median filter and a 3-D unsharp mask ($\sigma = 2$, weighting factor = 0.6). Then, we used SoilJ to automatically detect the coordinates of the aluminium walls. We calibrated all images to the same greyscale, by scaling the grey-values in each horizontal cross-section between the 0.1 percentile (depicting air-filled pores) and the value of the aluminium walls. This allowed us to average the histograms of all acquired images to a joint histogram. We used the minimum method on the joint histogram to segment the air-filled porosity from the remaining soil "matrix" voxels on all images, which obtained a grey-scale value of 8800. The soil matrix comprises soil solids and water-filled pores. The overwhelming majority of these water-filled pores will be of a size below image resolution, although at the larger pressure heads, the segmented matrix will also include some water films in larger (X-ray visible) pores. Moreover, we delineated POM from the images acquired at a pressure head of −30 cm by setting a lower threshold at a grey-scale value of 8800 and the larger one at 13000. The upper threshold was determined upon visual inspection in several images. Subsequently, we ran three consecutive 3-D erosion operations on the resulting binary image with a structural element with a one voxel large radius followed by three 3-D dilation steps with the same structuring element. In this fashion, we eliminated partial volumes from the segmented POM phase.

We extracted the volumetric air content (or air-filled porosity; cm^3 air cm^{-3} soil volume), the surface area of the air phase (cm^2 air surface cm^{-3} soil volume) and the surface area-to-volume ratio of the air phase (cm^2 air surface cm^{-3} air) of the imaged porosity from the binary images. We quantified the pore diameter distribution using the method of maximally inscribable spheres (Hildebrand and Rüegsegger, 1997). The fractal dimension of the interface between macropores and soil matrix was yielded by box counting. We also derived three measures of air connectivity, namely the air-filled porosity which is connected to the upper surface of the soil, the percolating air phase (i.e. that which is connected from the top to the bottom of the core) and the connection

Table 1
Bulk soil characteristics: bulk density (BD), organic carbon content (Org-C) and soil texture for the 8 cores used in the experiment. Averages and standard deviations (in brackets) for till and no-till cores are shown on the last rows together with significant differences between the two groups tested by one-way ANOVA (**bold *P*<0.05**). The row headed "field" shows representative data from field measurements with standard deviations between the different blocks. BD and C and N contents in 2015 at 10–20 cm depth and texture in 2009 at 0–30 cm depth (personal communication from Guillaume Vitte).

Treat.	Core	BD ($g\ cm^{-3}$)	Org-C (%)	Tot-N (%)	soil C/N ratio	Clay (%)	Silt (%)	Sand (%)
till	1	1.48	1.10	0.11	10.4	17.6	73.9	8.5
	2	***1.26***	*0.95*	*0.10*	*9.4*	***15.4***	*75.8*	***8.9***
	3	1.52	1.01	0.11	9.4	17.6	73.7	8.7
	4	1.42	1.11	0.11	9.9	17.1	74.9	8.0
no-till	5	1.53	0.95	0.12	8.2	21.4	72.6	6.0
	6	1.57	0.86	0.10	8.9	18.4	75.5	6.1
	7	1.59	0.93	0.11	8.8	20.9	72.9	6.1
	8	1.47	0.79	0.09	8.7	20.6	73.8	5.6
till	cores	1.42	1.04	0.11	9.8	16.9	74.6	8.5
		(0.11)	(0.08)	(0.00)	(0.5)	(1.1)	(1.0)	(0.4)
	field	1.42	1.09	0.10	10.5	20.4	72.7	7.0
		(0.02)	(0.10)	(0.01)	(0.9)	(2.1)	(3.9)	(2.3)
no-till	cores	1.54	0.88	0.10	8.7	20.3	73.7	6.0
		(0.05)	(0.07)	(0.01)	(0.3)	(1.3)	(1.3)	(0.3)
	field	*1.49*	*0.98*	*0.10*	*9.8*	*18.3*	*74.5*	*7.2*
		(0.02)	*(0.05)*	*(0.01)*	*(0.7)*	*(4.2)*	*(2.4)*	*(2.4)*
	Anova	*P=0.105*	***P=0.023***	*P=0.730*	***P=0.007***	***P=0.007***	*P=0.323*	***P<0.001***

probability, which is defined as the probability that two air-phase voxels are connected (Renard and Allard, 2013; Jarvis et al., 2017). Finally, we classified a fraction of the pore space imaged at a pressure head of −30 cm as biopores using the method described by Lucas et al. (2022), as implemented into SoilJ.

Finally, we calculated the distances of each soil matrix voxel to the nearest air-filled pore connected to the soil surface (Koestel and Schlüter, 2019). Moreover, we also mapped these distances onto each POM voxel by combining the distance map with the binary POM image. Note that we could not obtain the POM phase from the images acquired under wetter conditions because of ambiguities between grey-scale values of POM and water. We therefore carried out a rigid registration of the images collected at pressure heads of zero, −10 and −20 cm to the one acquired at −30 cm using the elastix software (Klein et al., 2010; Shamonin et al., 2014).

2.5. Statistical analyses

All statistical analyses were run using R software (R core team, 2023). Statistical differences between experimental treatments (*Till* and

Table 2
Metrics of X-ray visible porosity and particulate organic matter (POM) volume measured after equilibration at a pressure head of −30 cm at the base of the soil core (square brackets show the percentage connected porosity in relation to the total visible porosity). Averages and standard deviations (in brackets) for *till* and *no-till* cores are shown on the last rows together with P values for significant differences between the two groups tested by one-way ANOVA (**bold *P*<0.05**, data were log transformed to fulfil homoscedasticity).

		X-ray imaged air-filled porosity ($cm^3\ cm^{-3}$)			Surface area of the air phase ($cm^2\ cm^{-3}$)		Surface to volume ratio of the pore space (cm^{-1})					
Treat.	Core	Total	Connected to top	Connected to top and bottom	Total	Connected to top	Total	Connected to top	Connection probability Γ(-)	Biopores ($cm^3\ cm^{-3}$)	Biopore fraction of the pore space (%)	Total POM ($cm^3\ cm^{-3}$)
till	1	0.0326	0.0264 [81%]	0.0263 [81%]	1.681	1.160 [69%]	51.60	43.87 [85%]	0.65	0.0006	1.8	0.0038
	2	0.0887	0.0825 [93%]	0.0825 [93%]	4.346	3.632 [84%]	48.98	44.02 [90%]	0.86	0.0005	0.5	0.0022
	3	0.0237	0.0154 [65%]	0.0143 [60%]	1.366	0.608 [45%]	57.55	39.50 [69%]	0.36	0.0003	1.4	0.0025
	4	0.0425	0.0364 [86%]	0.0359 [84%]	2.281	1.666 [73%]	53.64	45.76 [85%]	0.71	0.0011	2.6	0.0037
no-till	5	0.0200	0.0140 [70%]	0.0137 [68%]	1.479	0.955 [65%]	74.08	71.33 [96%]	0.51	0.0010	5.3	0.0031
	6	0.0169	0.0087 [51%]	0.0059 [35%]	0.924	0.284 [31%]	54.54	32.66 [60%]	0.17	0.0040	23.7	0.0006
	7	0.0171	0.0106 [62%]	0.0102 [59%]	1.668	0.827 [50%]	97.52	78.21 [80%]	0.35	0.0009	5.3	0.0012
	8	0.0245	0.0155 [63%]	0.0152 [62%]	1.849	0.836 [45%]	75.49	54.02 [72%]	0.39	0.0019	7.7	0.0026
till	av	0.0469	0.0402	0.0397	2.418	1.766	52.94	43.29	0.65	0.0006	1.6	0.0031
	sd	(0.0289)	(0.0295)	(0.0298)	(1.340)	(1.317)	(3.61)	(2.66)	(0.21)	(0.0003)	(0.9)	(0.0008)
no-till	av	0.0196	0.0122	0.0112	1.480	0.726	75.41	59.05	0.35	0.0020	10.5	0.0019
	sd	(0.0035)	(0.0031)	(0.0041)	(0.400)	(0.300)	(17.57)	(20.33)	(0.14)	(0.0014)	(8.9)	(0.0012)
	anova	***P=0.043***	***P=0.034***	***P=0.038***	*P=0.228*	*P=0.146*	***P=0.035***	*P=0.240*	*P=0.061.*	*P=0.051.*	***P=0.011***	*P=0.159*

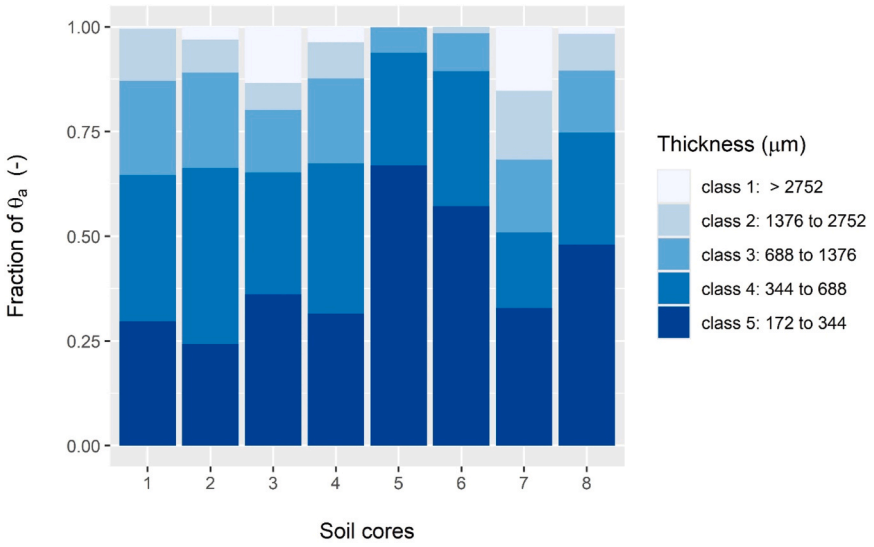

Fig. 1. Thickness distribution of the X-ray imaged porosity (θ_a) at a pressure head of −30 cm for all 8 cores (*tilled* cores are numbers 1–4, with an average median thickness of 507 μm and *no-till* cores are numbers 5–8 with an average median thickness of 398 μm). Thickness class 3 is more prevalent in tilled cores while class 5 is more prevalent in no-till cores ($P < 0.05$ tested by ANOVA).

no-till) for bulk soil properties, characteristics of the X-ray visible air phase and C emission rates were investigated with one-way ANOVA. Relationships between the X-ray imaged metrics of air and matrix phases and C emission rates were investigated by calculating Spearman rank correlation coefficients (ρ).

3. Results and discussion

3.1. Bulk characteristics of soil cores

Table 1 presents the results of measurements of bulk density on the soil cores as well as the texture analysis and measurements of C and N contents made on the disturbed and mixed soil from the cores after the conclusion of the drainage/incubation experiment. The eight cores sampled on the same field from four separate blocks under two contrasting tillage treatments showed rather homogeneous bulk characteristics. The textural analysis showing significantly higher clay contents and lower sand contents in cores from the *no-till* treatment, although differences were rather small (20 % clay and 6 % sand in *no-till* compared with 17 % and 8 % in the *till* treatment). The *no-till* plots had slightly higher bulk densities on average but these differences were not significant. Soil core 2 (from the *till* treatment) differed markedly from the others, with a much smaller bulk density, a smaller clay content and a correspondingly larger sand content. We could not identify any reason *a priori* to explain these differences from other sampling locations. Soil organic C and N contents were small (ranging from 0.86 % to 1.11 % for C and 0.09–0.12 % for N), as could be expected for an agricultural soil at a depth of 10–15 cm under intensive management (Vos et al., 2019). Slightly lower C contents and C to N ratios were found in the *no-till* soil cores compared to *the till* treatment (Table 1), which reflect differences

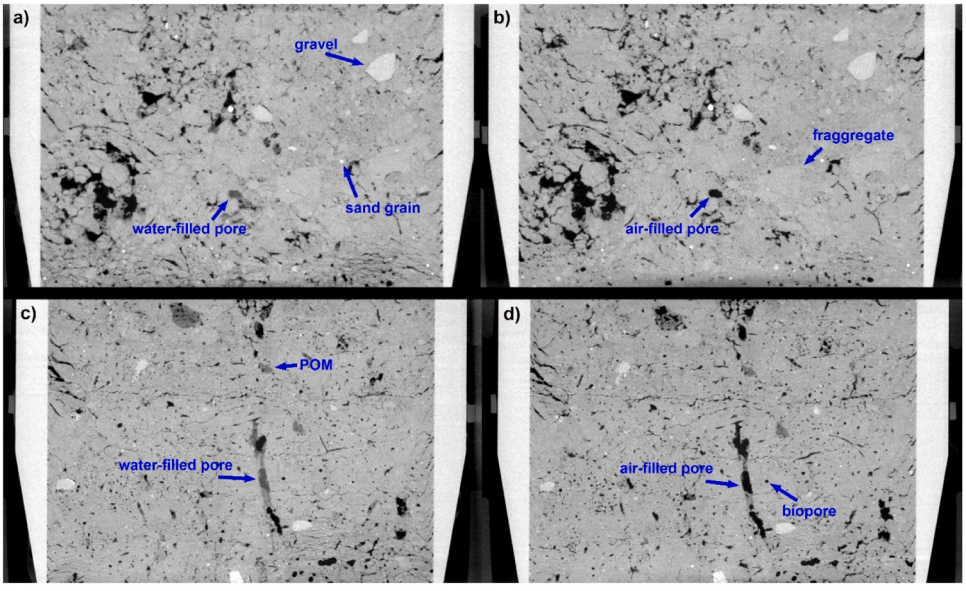

Fig. 2. Illustrative vertical cross-sections through 3D X-ray images of samples from the tilled (a and b) and no-till treatments (c and d). The samples are shown at saturation $\Psi_0 = 0$ cm (a and c) and a pressure head of $\Psi_{30} = -30$ cm (b and d). In the tilled sample, fragments and aggregates are discernible, while the no-till sample features numerous small rounded biopores. The drainage of some macropores between the two pressure head steps is also illustrated, with water-filled pores of a dark grey colour becoming air-filled (i.e. showing a black colour).

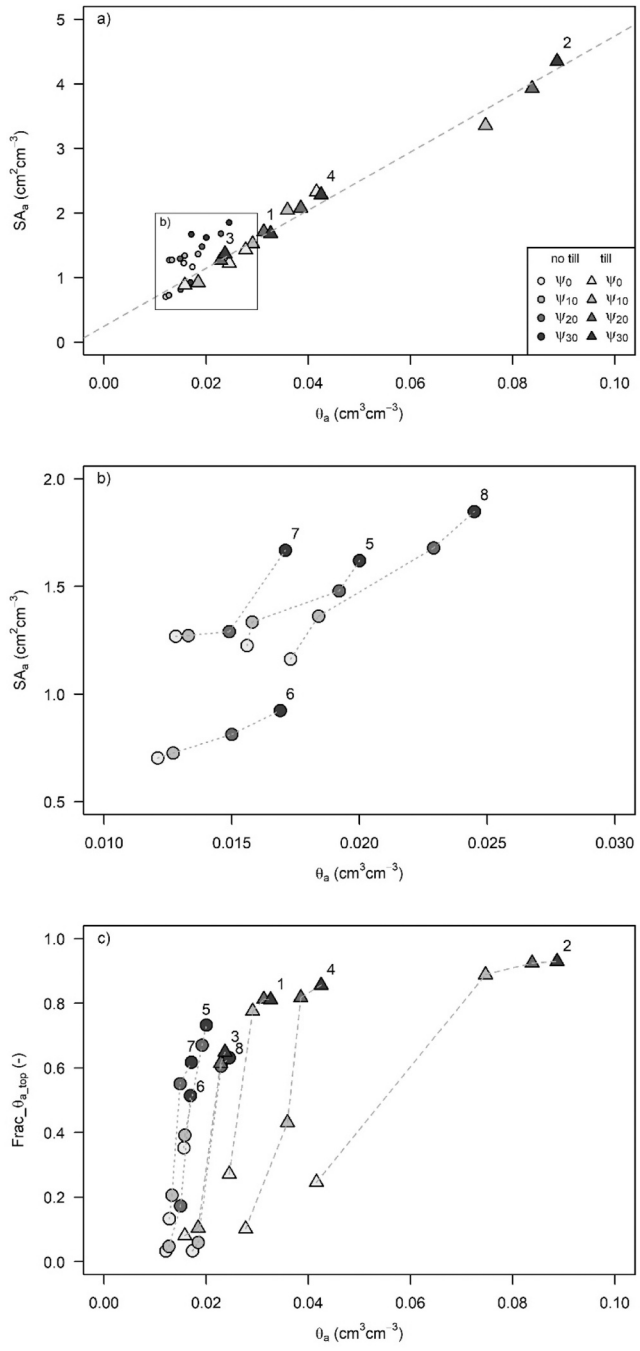

Fig. 3. The surface area of the total imaged air-filled porosity (SA_a, a and b) as well as the fraction of the imaged air-filled porosity that is connected to top (Frac_θ_{a_top}, c) as a function of the volumetric air content of the total imaged air-filled porosity (θ_a) for all pressure heads (Ψ_0 = 0 cm, Ψ_{10} = −10 cm, Ψ_{20} = −20 cm, Ψ_{30} = −30 cm) and all cores, cores 1–4: *till* (*triangles*) and cores 5–8: *no-till* (circles). Labels show the core number.

in the distribution of organic matter in the soil profile between the treatments (Dimassi et al., 2013).

3.2. Imaged pore network characteristics

The X-ray imaged porosity for the cores equilibrated at a pressure head of −30 cm varied from less than 2 % to up to 8 % (Table 2), with significantly larger values in the cores from the *till* treatment (with averages value of ca. 5 % and 2 % in *till* and *no-till* treatments respectively). Similar differences in structural porosity between conventionally-tilled and no-till soils have been noted in previous studies (e.g. Lipiec et al., 2006; Strudley et al., 2008).

These differences in the X-ray imaged porosity were also mirrored in the visible porosity connected to the soil surface and the percolating porosity (i.e. that connected to both the top and bottom of the core; Table 2) as all three measures were very strongly correlated (data not shown). The fraction of the imaged porosity connected to the top varied from 60 % to 93 % (core 2, outlier core with a much smaller bulk density, Table 1) for the cores from the *till* treatment, compared with 35–68 % in the case of the cores from the *no-till* treatment (Table 2). Except for one core from the *no-till* treatment (core 6), all cores with a visible pore network connecting to the upper surface also percolated (Table 2). The connection probability Γ was also generally larger in the tilled samples, although unlike the other two measures of connectivity, this difference between the treatments was not quite significant at $P = 0.05$.

In contrast to the X-ray imaged porosity, the surface area was not significantly different between treatments (Table 2). This was the case for both the total surface area and the part connected to the upper surface (Table 2). This suggests that the distribution of the pore space in the cores from the *no-till* treatment was significantly more heterogeneous and "space-filling" (*i.e.* exploring a larger volume of the total soil volume), something which can be expected as spatial variations in physical properties can be preserved when soils are not disturbed by tillage (Hubert et al., 2007). This is also illustrated by a higher fractal dimension found in the cores of the *no-till* treatment with an average value of 2.27 compared to 2.17 for the *till* cores (data not shown). This hypothesis is also supported by the fact that the surface area-to-volume ratio is significantly larger in the *no-till* treatment (Table 2) and by the broader size (thickness) distribution of the imaged pore networks in these undisturbed soils, with both a larger proportion of smaller pores (<344 μm) and more variation among the cores for all size classes than in the *till* treatment (Fig. 1).

Interestingly, and in accordance with the observations of a higher faunal activity at the sampling site, the fraction of the total X-ray visible porosity comprising biopores was significantly larger in the cores from the *no-till* treatment (Table 2). Again, core 6 with a less well-connected pore network, was very different from the other cores with an extremely large value of the biopore fraction. These overall treatment differences in the types of macropores are illustrated in the example vertical cross sections through the 3D X-ray images presented in Fig. 2, where the presence of numerous round biopores is visible in the no-till core, while several fragments or aggregates generated from tillage can be seen in the tilled core.

3.3. Development of the air phase during drainage from saturation to −30 cm pressure head

Fig. 3 shows that the soil cores were not fully saturated after the prewetting treatment in the water bath, as the imaged air-filled porosity was never smaller than 0.01 $cm^3\ cm^{-3}$. Examples of such air-filled pores can be seen coloured black in Fig. 2a,c. Fig. 3 also shows that a large proportion of this air in the samples at the start of the experiment (*i.e.* at the largest pressure heads and lowest imaged air-filled porosity) was not connected to the upper surface of the core. Thus, the procedure to initially saturate the samples from the base was not completely effective, as some air had become entrapped. Fig. 3 shows that the fraction of the air phase connected to the upper surface of the cores increased rapidly as the soil began to drain and air entered from the soil surface. This is partly because air entering the soil during the experiment must be connected to the surface, but also because it may connect to some of the initially isolated air pockets. The proportion of the air phase which was disconnected from the upper surface of the cores varied from 65 % to 97 % close to saturation and between 7 % and 49 % after drainage had ceased at the smallest pressure head (-30 cm). The non-linear relationship between the connected air fraction and the volumetric air content

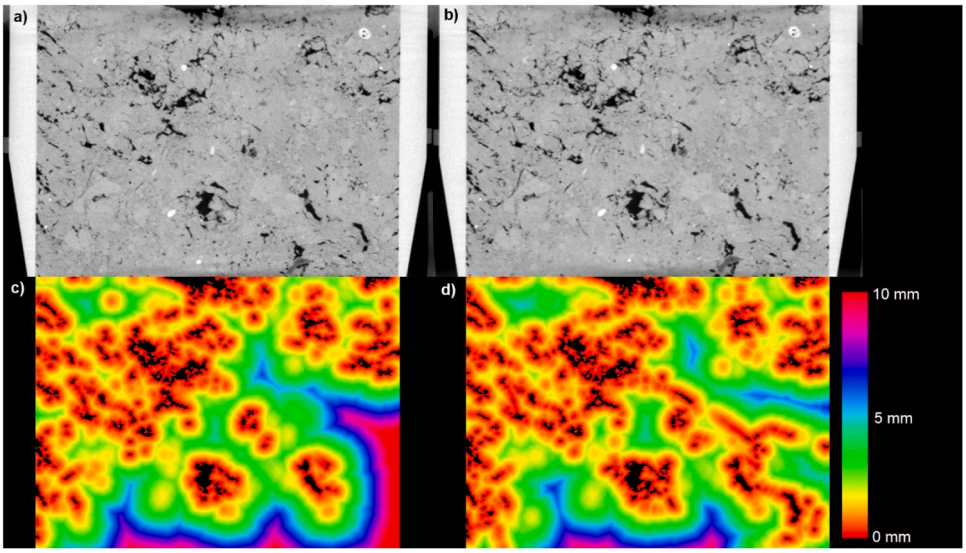

Fig. 4. Vertical cross-sections of two X-ray images of one of the tilled samples (core 1) equilibrated at Ψ_{10} = -10 cm (a) and Ψ_{30} = -30 cm (b) pressure head, and the corresponding maps of the distance (s) from a matrix voxel to the closest voxel belonging to the air-filled porosity connected to the top (c and d).

shown in Fig. 3 is to be expected according to percolation theory (e.g. Jarvis, et al., 2017; Koestel et al., 2018). Overall, the process of drainage of larger structural pores, examples of which can be seen in Fig. 2, resulted in a reasonably well-connected network of air-filled porosity at the final pressure head of – 30 cm, especially in the tilled treatment (see Table 2 and Fig. 3). However, for smaller air-filled porosities, the fraction of the air phase connected to the upper surface is somewhat larger in the no-till cores, which may suggest that air-entry into the larger pores of the undisturbed no-till soil during the initial stages of drainage was more effective in establishing "re-connections" with the initially entrapped air. As expected, the air content connected to the upper surface of the core was strongly correlated with both the connection probability (ρ=0.94) and the percolating air content (ρ=0.97; data not shown).

Fig. 3(a and b) also shows how the surface area of the air-filled porosity (SA_a) increases concomitantly with volumetric air contents during the drainage process. Indeed, these two variables are very strongly correlated (Fig. 3). The relationship has a steeper slope in the case of the cores from the *no-till* treatment, which means that the surface-to-volume ratio of the air is larger (see also Table 2) at any pressure head in these cores compared to the cores from the tilled treatment. This indicates a more heterogeneous "space-filling" pore

Table 3
Minimal and maximal C emission rates and the respective pressure heads at which it was measured for each core (left part of the table), as well as the related imaged air-filled porosity connected to the top, the corresponding specific surface area (* of the air-filled porosity connected to top) and the volume of the matrix at a distance s < 2.37 mm from the imaged air-filled porosity connected to the top (**, middle part of the table). The C emissions expressed per volume or surface of the imaged air-filled porosity connected to top (*) are presented in the right part of the table. Averages and standard deviations (in brackets) for *till* and *no-till* cores are shown on the last rows together with significant differences between the two groups tested by ANOVA (**bold *P* < 0.05**) for values measured at contrasting pressure heads (0 and −20 cm or −30 cm).

Treat.	Core	Ψ	C emission rates C_{em}	Air-filled porosity connected to top	Specific surface area*	Matrix volume at s<2.37mm**	C_{em} per volume of air*	C_{em} per surface area of air*
		(cm)	(μg C-CO_2 g C^{-1} h^{-1})	(cm^3 cm^{-3})	(cm^2 cm^{-3})	(cm^3 cm^{-3})	(μg C-CO_2 g C^{-1} h^{-1} cm^{-3})	(μg C-CO_2 g C^{-1} h^{-1} cm^{-2})
till	1	0	30.4	0.0067	0.189	0.06	32	170
		-30	43.2	0.0264	1.160	0.58	12	10
	2	0	38.7	0.0102	0.345	0.10	027	77
		-30	65.4	0.0825	3.632	0.96	6	2
	3	0	21.0	0.0013	0.053	0.05	116	2198
		-20	51.8	0.0140	0.513	0.36	26	51
	4	0	18.2	0.0028	0.099	0.08	45	458
		-20	44.3	0.0315	1.440	0.73	10	7
no-till	5	0	41.5	0.0055	0.375	0.17	53	141
		-20	62.9	0.0141	0.949	0.68	31	33
	6	0	13.2	0.0006	0.046	0.07	161	3474
		-20	37.8	0.0026	0.150	0.15	103	682
	7	0	26.4	0.0017	0.144	0.10	109	758
		-30	42.6	0.0106	0.827	0.60	28	34
	8	0	19.7	0.0006	0.040	0.06	236	5937
		-20	60.2	0.0139	0.701	0.63	31	44
till		*0*	27.1 (9.4)	0.0053(0.004)	0.172 (0.129)	0.07 (0.02)	55 (41)	726 (995)
		-20 / -30	51.2 (10.2)	0.0386 (0.0302)	1.686 (1.354)	0.66 (0.25)	13(9)	17 (23)
no till		*0*	25.2 (12.1)	0.0021 (0.0023)	0.151 (0.157)	0.10 (0.05)	140 (78)	2578 (2667)
		-20 / -30	50.9 (12.5)	0.0103 (0.0054)	0.657 (0.352)	0.52 (0.25)	48 (39)	198 (323)
	Anova	*0*	*P = 0.815*	*P = 0.223*	*P = 0.848*	*P = 0.328*	*P = 0.104*	*P = 0.241*
		-20 / -30	*P = 0.972*	*P = 0.052*	*P = 0.192*	*P = 0.445*	*P = **0.027***	*P = 0.077.*

Table 4
Spearman rank correlation coefficients between C emission rates (μg CO_2 g C^{-1} h^{-1}) and the total imaged air-filled porosity or the imaged air-filled porosity connected to the top (cm^3 cm^{-3}) as well as with the specific surface area of the imaged air-filled porosity or the imaged air-filled porosity connected to top (cm^{-1}) and with the matrix volume (cm^3 matrix cm^{-3} soil volume) at a distance of < 2.37 mm from the interface with the imaged air-filled porosity connected to top. Significant correlations are indicated in bold (* $P < 0.05$). The number of scans vary per group: (i) ***overall*** considers all measurements (all, n = 32, per treatment, n = 16), (ii) ***between cores*** considers one pressure head at a time (all, n = 8, per treatment, n = 4).

			Air content θ_a		Surface area SA_a		Active matrix volume $\theta_{mat,active}$	POM in active zone $\theta_{POM,\ active}$
			Total	Connected to top	Total	Connected to top		
	Treat.	Ψ (cm)	(cm^3 cm^{-3})		(cm^2 cm^{-3})		(cm^3 cm^{-3})	(cm^3 cm^{-3})
Overall	*all*	-	**0.493**	**0.689**	**0.599**	**0.743**	**0.805**	**0.695**
	till	-	**0.510**	**0.714**	**0.540**	**0.707**	**0.712**	**0.432**
	no-till	-	**0.774**	**0.840**	**0.815**	**0.877**	**0.835**	**0.874**
Between cores	*all*	0	0.238	**0.786**	0.548	**0.881**	0.619	0.667
(for each pressure head)		-10	0.524	0.476	0.333	0.476	0.381	0.619
		-20	0.429	0.524	0.476	0.500	**0.714**	0.476
		-30	0.571	0.571	0.500	0.571	0.635	0.513
	till	0	0.400	0.800	0.400	0.800	0.400	0.400
		-10	0.200	0.400	0.200	0.400	0.400	0.000
		-20	0.400	0.400	0.400	0.400	0.400	-0.400
		-30	0.400	0.400	0.400	0.400	0.400	-0.800
	no-till	0	0.400	**1.000**	**1.000**	0.800	0.800	0.800
		-10	0.800	0.800	0.400	0.800	0.400	**1.000**
		-20	0.600	**1.000**	0.800	**1.000**	**1.000**	**1.000**
		-30	0.800	0.800	0.400	**1.000**	0.800	**1.000**

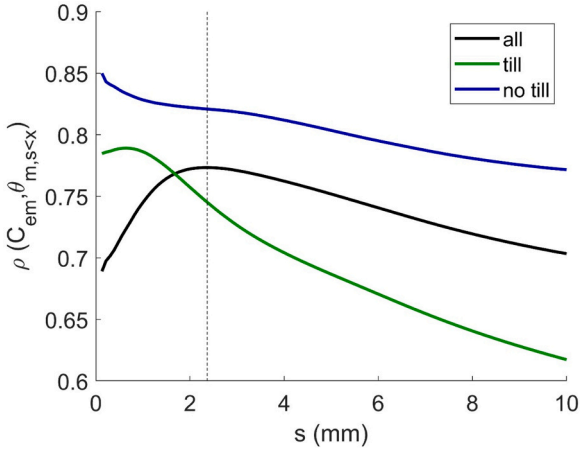

Fig. 5. Spearman correlation coefficients between C emission rates (C_{em}, μg C-CO_2 g^{-1} soil C h^{-1}) and the matrix volume $\theta_{m,s<x}$ (cm^3 matrix cm^{-3} soil volume) located at a distance to the nearest surface-connected air-filled voxel less than a threshold distance s (mm), plotted as a function of s, for all cores together and for each treatment separately (see legend). A maximum correlation coefficient is found at s = 2.37 mm.

structure, which is also in line with the predominance of air-filled pores of smaller diameter (Fig. 1) in the cores from the *no-till* treatment. The relationships in Fig. 3 are also less linear for the no-till cores, which may suggest a more heterogeneous diameter size distribution of the air phase (see Fig. 1), as also found by Kravchenko et al. (2011) and Wang et al. (2012). The relation between surface area and volume was also strikingly similar for all intact cores from the *till* treatment (i.e. they were all aligned on the same regression line), whereas the relationships for the cores from the *no-till* treatment were more heterogeneous among cores (Fig. 3b). This is presumably the result of a spatially heterogeneous soil structure arising from biological activity, in comparison with a soil structure that has been repeatedly homogenized by tillage fragmentation and reconsolidation (Hubert et al., 2007).

Fig. 4 shows an example of how air-entry during the drainage process changes the volume of the soil matrix located within different distances to the interface with the air connected to the soil surface. For example, as the air content increases as a consequence of a decrease in the pressure head from −10 (left-hand figure) to −30 cm (right-hand figure), the volume of the soil matrix located within 2 mm of the interface to the connected air phase increases, while the volume of the matrix located further away from the interface diminishes.

3.4. Carbon dioxide emissions and relationships with the air-filled porosity and POM

Measured carbon emission rates varied from 13.2 μg CO_2 g C^{-1} h^{-1} for one *no-till* core equilibrated at saturation (core 6) to 65.4 μg CO_2 g C^{-1} h^{-1} for one *till* core (core 2) equilibrated at a pressure head of −30 cm (Table 3). A relatively large variation in C emission rates among individual replicate cores was found resulting in no significant difference between the treatments overall (Table 3). C emission rates were positively and significantly correlated with the total X-ray imaged air-filled porosity and its surface area (Table 4), but the air-filled porosity connected to the soil surface and the corresponding surface area were even better predictors, with correlation coefficients of 0.501 and 0.687 for the porosity (total and connected to top) and 0.599 and 0.743 for the surface area respectively (Table 4). Fig. 5a shows that a thickness of 2.37 mm for the soil matrix volume in contact with the matrix/air interface gave the strongest correlation with C emission rates. We therefore make use of this distance as a proxy to estimate an "active" soil volume (Schlüter et al., 2024) which should be responsible for much of the microbial production of CO_2 under the current experimental conditions. Our result is within the range of values found in a meta-analysis of denitrification experiments comprising 89 datasets taken from 27 studies (Schlüter et al., 2024).

We found that the active matrix volume was the best predictor of C emission rates overall, with a coefficient of 0.801 (Table 4). This was especially the case for the cores of the *till* treatment, implying that POM, although very important, is not the only source of C for emissions. In contrast, the air-filled porosity and its specific area, as well as the volume of POM in the active zone were equally good or better predictors for the cores from the *no-till* treatment. Simple calculations (not shown here, but assuming an average SOM density of 1.2 g cm^{-3} and that SOC is 50 % of SOM) based on the measured organic carbon contents and bulk densities (Table 1) suggest that the total X-ray imaged POM (see Table 2) amounts to ca. 10 % of the total soil organic carbon stocks in both treatments. Nevertheless, the strong correlations of C emissions with POM, especially in the no-till treatment, suggests that either POM was a dominant source of C for the emissions measured in our short

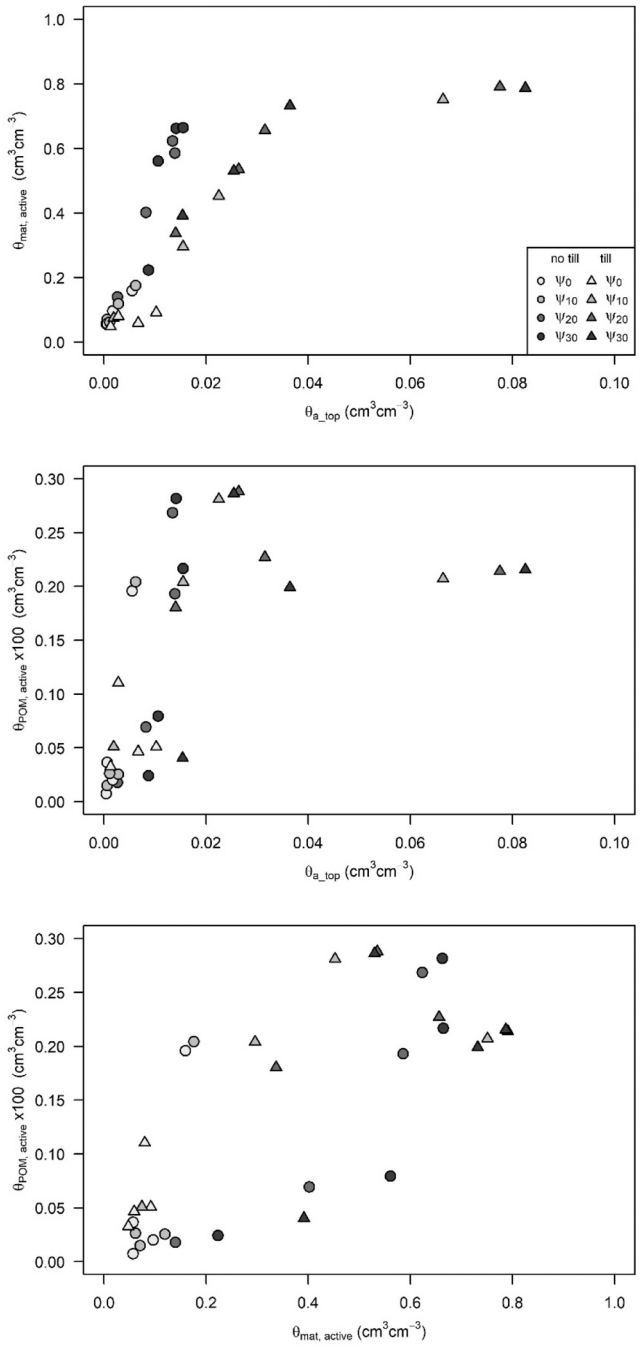

Fig. 6. The soil matrix volume within 2.37 mm of an air-filled voxel connected to the soil surface ($\theta_{m,s<2.37\ mm}$, cm^3 matrix cm^{-3} soil volume, referred as the "*active soil matrix*", a), and the volume of POM within this *active soil matrix* (cm^3 SOM cm^{-3} soil volume, b) plotted as a function of the imaged air-filled porosity connected to the soil surface (θ_{a_top}), as well as the volume of POM plotted as a function of the *active soil matrix* volume (c) for all pressure heads ($\Psi_0 = 0$ cm, $\Psi_{10} = -10$ cm, $\Psi_{20} = -20$ cm, $\Psi_{30} = -30$ cm) and all cores, cores 1–4: *till* (*triangles*) and cores 5–8: *no-till* (circles).

incubations or that it was spatially correlated with other sources of C, or both.

Fig. 6 together with Fig. 3, shows that all four of these potential predictors of CO_2 emissions are strongly correlated. This is not surprising: as air enters the pore space during drainage, the air-filled porosity increases along with the fraction that is connected to the surface, as isolated air clusters merge with the main (connected) cluster. As a natural consequence of this expanding network of air-filled pores connected to the soil surface, both the area of the connected air-soil matrix interface and the (presumably) aerobic volume of the matrix located within a given distance of this interface must also increase, as will the amount of POM. We expect CO_2 emissions under wet soil conditions to be regulated by this potentially active soil volume for aerobic microbial activity and the POM it contains, as well as by the air-filled porosity supporting diffusive gas transport to and from the soil surface (Skopp et al., 1990). During drainage, diffusion and O_2 availability become less limiting and the balance between O_2 demand and supply should become more favourable (e.g. Lacroix et al., 2021). Thus, Fig. 7a-d shows how CO_2 emission rates increased as the connected air-filled porosity, the active matrix volume, the surface area of the interface between the two and the amount of POM in the active zone all increased as the soil cores were drained from saturation to smaller pressure heads.

Combining both treatments, CO_2 emissions correlated best with the surface area of the interface under very wet conditions at and close to saturation (*i.e.* for values of surface area less than ca. 0.5 cm^{-1}, Fig. 7b and Table 4, ρ=0.881). This agrees with theoretical studies that suggest that the air-water interfacial area, which affects diffusion in both air and water and thus the availability of O_2 to the microbes should be one of the major factors limiting C emissions in wet soils close to saturation (Huang et al., 2023). Under these conditions, the surface area of the air phase represents the interface between the remaining microbially active microsites (e.g. Heitkötter and Marschner, 2018b, Leue et al., 2021) and the air-filled diffusion pathways connected to the soil surface. Moving further away from saturated conditions (i.e. at pressure heads of −20 cm and −30 cm), the active POM volume rather than the air-filled porosity was the best predictor of C emission rates overall (Table 4; Fig. 7d), suggesting that gas diffusion and oxygen limitation no longer limited microbial activity and C emissions, which were now more limited by substrate availability (Schlüter et al., 2022). Note that using C emission rates expressed per gram of soil (Table S1) instead of g of soil C in the calculation of the correlation coefficients did not change the se results.

The form of the relationships between C emissions and air content or surface area shown in Fig. 7a,b differs between the two treatments, with a steeper slope in the case of *no-till* cores. Thus, C emissions tend to be larger from *no-till* soil for any given air content and surface area of interface (see also Table 3). This result can be explained by Fig. 6a,b, which show that both the active matrix volume and the volume of POM it contains increase faster in the *no-till* soil as the air content increases during drainage. This is further evidence of the more heterogeneous and "space-filling" soil macropore structure that has developed in the treatment undisturbed by tillage. Fig. 6c suggests that the *no-till* cores do not contain more POM in the active zone than the till cores. However, there may also be differences between the two treatments in the spatial distributions of sources of C substrate of different qualities as well as microbial communities, as these also determine C emissions from soil (e.g. Heitkötter and Marschner, 2018a) and are known to be highly heterogeneous (e.g. Pankhurst et al., 2002, Nunan et al., 2003; Patel et al., 2021; Peth et al., 2014; Rawlins et al., 2016, Zheng et al., 2022). It is possible that the active zone close to the air-filled porosity connected to the surface of the *no-till* cores that drains close to saturation contains more C and exhibits a greater microbial activity under the present experimental conditions, as a consequence of the larger fraction of biopores (Table 2; see Bundt et al., 2001; Hoang et al., 2016; Athmann et al., 2017).

4. Conclusions

To our knowledge, this is the first laboratory experiment that couples repeated X-ray measurements quantifying how the soil air phase develops in soils of intact structure during drainage from saturation with measurements of C emission rates in soil cores of contrasted structures arising from different soil tillage management. We acknowledged the importance of C emissions close to saturation due to entrapped air and to some remaining biologically active sites in the soil as well as connected

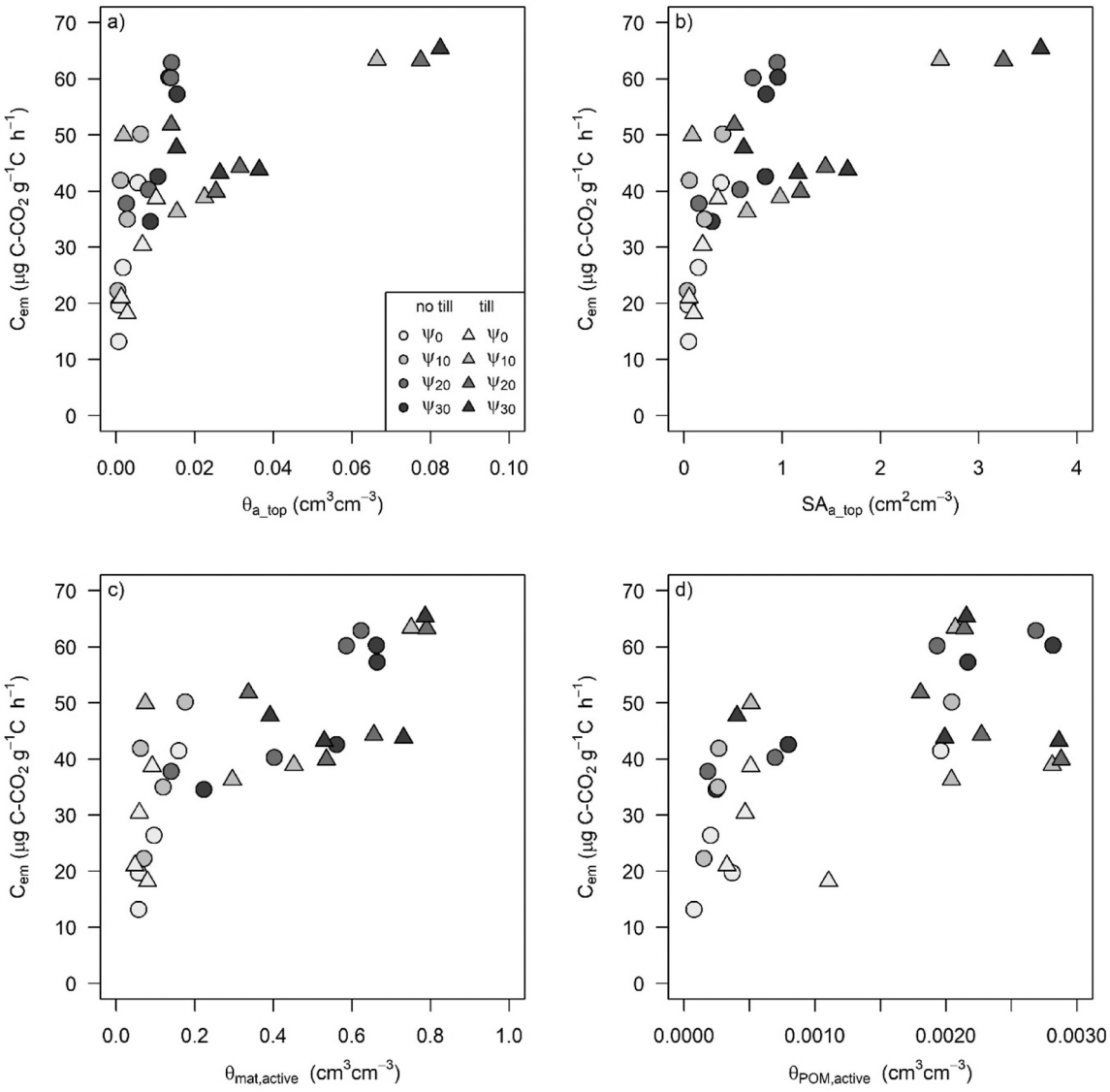

Fig. 7. C emission rates (C_{em}) measured on each core (triangles: *till (*cores 1–4,); circles: *no-till* (cores 5–8) and each pressure head ($\Psi_0 = 0$ cm, $\Psi_{10} = -10$ cm, $\Psi_{20} = -20$ cm, $\Psi_{30} = -30$ cm) as a function of the imaged air-filled porosity connected to the top (θ_{a_top}, a), the corresponding specific surface area of the connected air-filled porosity (b), the volume of the *active soil matrix* in contact with the imaged air-filled porosity connected to the top located at a distance $s < 2.37$ mm from the interface (cm^3 matrix cm^{-3} soil volume, c) and the volume of POM within this active soil matrix (cm^3 POM cm^{-3} soil volume, d). Spearman correlation coefficients between the paired variables are shown in Table 4.

pathways through the soil pore space in structured soil that allow gas transport to and from the soil surface even when the air content is very small. This was especially true for soil cores from a *no-till* treatment that contained a larger proportion of biopores. As the cores were drained stepwise to a pressure head of −30 cm, increases in CO_2 emissions were found to be strongly correlated with the increase in the air-filled porosity connected to the soil surface as well with the volume of the soil matrix within a distance of ca. 2–3 mm of this connected air phase and the POM located in this active zone. We also found a stronger response of C emissions to increases in the air-filled porosity in the *no-till* cores and higher C emission rates for a smaller volume of air that we attribute to a more heterogeneous "space-filling" pore structure in the undisturbed cores, such that the pore size distribution is shifted towards smaller pores that allow air to enter within a larger part of the soil matrix, thereby connecting to more of the soil C in an active soil zone. We also showed that a larger proportion of these air-filled macropores were of biological origin in the *no-till* cores, which may also have been a factor contributing to greater C emissions at a given air content, as they may be more microbially active and spatially related to sources of soil C.

These results are important for an improved understanding of C emissions from wet soils close to saturation and how the response of C emissions to changes in soil moisture is affected by soil structure. Near-saturated conditions are not uncommon in soils, for example, in subsoils, especially at sites with shallow water tables. Our results should also be relevant in topsoil, for example following heavy rainfall in autumn, when soils are re-wetting and temperatures are not yet limiting microbial activity, and for certain type of agro-ecosystems such as paddy rice.

We did not attempt to derive empirical functions relating the response of C emissions to soil structure metrics at soil moisture contents close to saturation from this experiment. Nor did we test any theoretical functions using our data. This is because the number of soil cores was limited and the variations in both soil structure metrics and organic carbon contents among the samples were small. There is therefore a need in the future to investigate soils of more strongly contrasting structure and organic matter contents and distributions. This should help to support the development of improved models of soil organic matter turnover that could be useful in larger Earth System Models, not least in the context of climate change studies.

Funding sources

This research has been funded by the Swedish Research Council for Sustainable Development (FORMAS, grant 2018–00425).

Declaration of Competing Interest

We declare no conflicts of interest.

Acknowledgements

Soil cores were sampled at the long-term observatory for environmental research SOERE-ACBB (Système d'Observation et d'Expérimentation sur le long terme pour la recherche sur l'environnement – Agroecosystèmes, Cycles Biogéochimiques et Biodiversité, https://www.soere-acbb.com/) of INRAe (Institut National de Recherche en Agronomie et Environment). We would like to thank Guillaume Vitte and Frida Keuper (in charge of the technical and scientific board of the site) and the rest of the team for their welcome, advice and guidance, as well as site preparation before sampling. Special thanks to Bertrand Chauchard and Guillaume Vitte for helping us with soil core sampling. We are grateful to Stefano Manzoni (Stockholm University) for meaningful comments on the manuscript as well to the two anonymous reviewers.

Appendix A. Supporting information

Supplementary data associated with this article can be found in the online version at doi:10.1016/j.still.2025.106468.

Data availability

Data will be made available on request.

References

Alskaf, K., Mooney, S.J., Sparkes, D.L., Wilson, P., Sjögersten, S., 2021. Short-term impacts of different tillage practices and plant residue retention on soil physical properties and greenhouse gas emissions. Soil Tillage Res. 206 (October 2020).

Ananyeva, K., Wang, W., Smucker, A., Rivers, M., Kravchenko, A., 2013. Can intra-aggregate pore structures affect the aggregate's effectiveness in protecting carbon? Soil Biol. Biochem. 57, 868–875.

Athmann, M., Kautz, T., Banfeld, C., et al., 2017. Six months of L. terrestris L. activity in root-formed biopores increases nutrient availability, microbial biomass and enzyme activity. Appl. Soil Ecol. 120, 135–142.

Baveye, P.C., Otten, W., Kravchenko, A., Balseiro-Romero, M., Beckers, É ., Chalhoub, M., Darnault, C., Eickhorst, T., Garnier, P., Hapca, S., Kiranyaz, S., Monga, O., Mueller, C.W., Nunan, N., Pot, V., Schlüter, S., Schmidt, H., Vogel, H.J., 2018. Emergent properties of microbial activity in heterogeneous soil microenvironments: different research approaches are slowly converging, yet major challenges remain. Front. Microbiol. 9, 1–48.

Boizard, H., Yoon, S.-W., Leonard, J., Lheureux, S., Cousin, I., Roger-Estrade, J., Richard, G., 2013. Using a morphological approach to evaluate the effect of traffic and weather conditions on the structure of a loamy soil in reduced tillage. Soil Tillage Res. 127, 34–44.

Bouckaert, L., Sleutel, S., Loo, D.Van, Brabant, L., Cnudde, V., Hoorebeke, L.Van, Neve, S. De, Bouckaert, L., Sleutel, S., Loo, D.Van, Brabant, L., Cnudde, V., Hoorebeke, L.Van, Neve, S.De, 2013. Carbon mineralisation and pore size classes in undisturbed soil cores. Soil Res. 51 (1), 14–22.

Braakhekke, M.C., Beer, C., Hoosbeek, M.R., Reichstein, M., Kruijt, B., Schrumpf, M., Kabat, P., 2011. Somprof: a vertically explicit soil organic matter model. Ecol. Model. 222 (10), 1712–1730.

Bundt, M., et al., 2001. Preferential flow paths: biological 'hot spots' in soils. Soil Biol. Biochem. 33, 729–738.

Certini, G., Scalenghe, R., 2023. The crucial interactions between climate and soil. Sci. Total Environ. 856, 159169.

Chakrawal, A., Herrmann, A.M., Koestel, J., Jarsjö, J., Nunan, N., Kätterer, T., Manzoni, S., 2020. Dynamic upscaling of decomposition kinetics for carbon cycling models. Geosci. Model Dev. 13 (3), 1399–1429.

Chapman, S.B., 1971. A Simple Conductimetric Soil Respirometer for Field Use. Oikos 22 (3), 348–353. https://doi.org/10.2307/3543857.

Chatterjee, A., Taylor, J.M., Strauss, A., Locke, M.A., 2024. Soil carbon mineralization, enzyme activities, and crop residue decomposition under varying soil moisture regimes. Soil Sci. Soc. Am. J. 88 (1), 43–55.

Curiel Yuste, J., Baldocchi, D.D., Gershenson, A., Goldstein, A., Misson, L., Wong, S., 2007. Microbial soil respiration and its dependency on carbon inputs, soil temperature and moisture. Glob. Change Biol. 13 (9), 2018–2035.

Dimassi, B., Cohan, J.P., Labreuche, J., Mary, B., 2013. Changes in soil carbon and nitrogen following tillage conversion in a long-term experiment in Northern France. Agric., Ecosyst. Environ. 169, 12–20.

Doetterl, S., Stevens, A., Six, J., Merckx, R., Van Oost, K., Casanova Pinto, M., Casanova-Katny, A., Muñoz, C., Boudin, M., Zagal Venegas, E., Boeckx, P., 2015. Soil carbon storage controlled by interactions between geochemistry and climate. Nat. Geosci. 8 (10), 780–783.

Evans, S., Allison, S, D., Hawkes, C, V., 2022. Microbes, memory and moisture: predicting microbial moisture responses and their impact on carbon cycling. Funct. Ecol. 36 (6), 1430–1441.

Feng, Y., Wang, H., Liu, W., Sun, F., 2023. Global soil moisture–climate interactions during the peak growing season. J. Clim. 36 (4), 1187–1196.

Franzluebbers, A.J., 2002. Soil organic matter stratification ratio as an indicator of soil quality. Soil Tillage Res. 66 (2), 95–106.

Gabrielle, B., Mary, B., Roche, R., Smith, P., Gosse, G., 2002. Simulation of carbon and nitrogen dynamics in arable soils: A comparison of approaches. Eur. J. Agron. 18 (1–2), 107–120.

Garten, C.T., Classen, A.T., Norby, R.J., 2009. Soil moisture surpasses elevated CO2 and temperature as a control on soil carbon dynamics in a multi-factor climate change experiment. Plant Soil 319 (1–2), 85–94.

Ghosh, T., Maity, P.P., Das, T.K., Krishnan, P., Chakraborty, D., Bhatia, A., Ray, M., Kundu, A., Bhattacharyya, R., 2022. Characterization of soil pores through X-ray computed microtomography and carbon mineralization under contrasting tillage and land configurations in the Indo-gangetic plains of India. Front. Environ. Sci. 10 (May), 1–12.

González-Domínguez, B., Niklaus, P.A., Studer, M.S., Hagedorn, F., Wacker, L., Haghipour, N., Zimmermann, S., Walthert, L., McIntyre, C., Abiven, S., 2019. Temperature and moisture are minor drivers of regional-scale soil organic carbon dynamics. Sci. Rep. 9 (1), 6422.

Heitkötter, J., Marschner, B., 2018a. Is there anybody out there? Substrate availability controls microbial activity outside of hotspots in subsoils. Soil Syst. 2 (2), 1–12.

Heitkötter, J., Marschner, B., 2018b. Soil zymography as a powerful tool for exploring hotspots and substrate limitation in undisturbed subsoil. Soil Biol. Biochem. 124 (June), 210–217.

Helliwell, J.R., Sturrock, C.J., Grayling, K.M., Tracy, S.R., Flavel, R.J., Young, I.M., Whalley, W.R., Mooney, S.J., 2013. Applications of X-ray computed tomography for examining biophysical interactions and structural development in soil systems: a review. Eur. J. Soil Sci. 64, 279–297.

Henryson, K., Sundberg, C., Kätterer, T., Hansson, P.-A., 2018. Accounting for long-term soil fertility effects when assessing the climate impact of crop cultivation. Agric. Syst. 164, 185–192.

Herbst, M., Tappe, W., Kummer, S., Vereecken, H., 2016. The impact of sieving on heterotrophic respiration response to water content in loamy and sandy topsoils. Geoderma 272, 73–82.

Hildebrand, T., Rüegsegger, P., 1997. A new method for the model-independent assessment of thickness in three-dimensional images. J. Microsc. 185, 67–75. https://doi.org/10.1046/j.1365-2818.1997.1340694.x.

Hoang, D.T.T., Pausch, J., Razavi, B.S., et al., 2016. Hotspots of microbial activity induced by earthworm burrows, old root channels, and their combination in subsoil. Biol. Fertil. Soils 52, 1105–1119.

Huang, Z., Liu, Y., Huang, P., Li, Z., Zhang, X., 2023. A new concept for modelling the moisture dependence of heterotrophic soil respiration. Soil Biol. Biochem. 185, 109147.

Hubert, F., Hallaire, V., Sardini, P., Caner, L., Heddadj, D., 2007. Pore morphology changes under tillage and no-tillage practices. Geoderma 142 (1–2), 226–236.

Hursh, A., Ballantyne, A., Cooper, L., Maneta, M., Kimball, J., Watts, J., 2017. The sensitivity of soil respiration to soil temperature, moisture, and carbon supply at the global scale. Glob. Change Biol. 23 (5), 2090–2103.

IPCC. (2021). Summary for Policymakers. Page Climate Change 2021: The Physical Science Basis. Contribution of Working Group I to the Sixth Assessment Report of the Intergovernmental Panel on Climate Change [e [Masson-Delmotte, V., P. Zhai, A. Pirani, S.L.

Jarvis, N., Larsbo, M., Koestel, J., 2017. Connectivity and percolation of structural pore networks in a cultivated silt loam soil quantified by X-ray tomography. Geoderma 287, 71–79.

Jungkunst, H.F., Göpel, J., Horvath, T., Ott, S., Brunn, M., 2022. Global soil organic carbon–climate interactions: Why scales matter. Wiley Interdiscip. Rev.: Clim. Change 13 (4), 1–17.

Klein, S., Staring, M., Murphy, K., Viergever, M.A., Pluim, J.P.W., 2010. Elastix: A toolbox for intensity-based medical image registration. IEEE Trans. Med. Imaging 29 (1), 196–205.

Koestel, J., 2018. SoilJ: an ImageJ plugin for the semiautomatic pro cessing of three dimensional x-ray images of soils. Vadose Zone J.

Koestel, J., Dathe, A., Skaggs, T.H., Klakegg, O., Ahmad, M.A., Babko, M., Giménez, D., Farkas, C., Nemes, A., Jarvis, N., 2018. Estimating the permeability of naturally structured soil from percolation theory and pore space characteristics imaged by X-ray. Water Resour. Res. 54 (11), 9255–9263.

Koestel, J., Schlüter, S., 2019. Quantification of the structure evolution in a garden soil over the course of two years. Geoderma 338, 597–609.

Krause, H., Stehle, B., Mayer, J., Mayer, M., Steffens, M., Mäder, P., Fliessbach, A., 2022. Biological soil quality and soil organic carbon change in biodynamic, organic, and conventional farming systems after 42 years. Agron. Sustain. Dev. 42 (6).

Kravchenko, A., Guber, A., 2017. Soil pores and their contributions to soil carbon processes. Geoderma 287, 31–39.
Kravchenko, A.N., Wang, A.N.W., Smucker, A.J.M., Rivers, M.L., 2011. Long-term differences in tillage and land use affect intra-aggregate pore heterogeneity. Soil Sci. Soc. Am. J. 75 (5), 1658–1666.
Kuzyakov, Y., Blagodatskaya, E., 2015. Microbial hotspots and hot moments in soil: concept & review. Soil Biol. Biochem. 83, 184–199.
Lacroix, E.M., Rossi, R.J., Bossio, D., Fendorf, S., 2021. Effects of moisture and physical disturbance on pore-scale oxygen content and anaerobic metabolisms in upland soils. Sci. Total Environ. 780, 146572.
Lal, R., 2013. Intensive agriculture and the soil carbon pool. J. Crop Improv. 27, 735–751.
Lamichhane, J.M., Boizard, H., Dürr, C., Richard, G., Boiffin, J., 2021. Effect of cropping systems and climate on soil physical characteristics, field crop emergence and yield: a dataset from a 19-year field experiment. Data Brief. 39. https://doi.org/10.1016/j.dib.2021.107581.
Leue, M., Holz, M., Gerke, H.H., Taube, R., Puppe, D., Wirth, S., 2021. Spatially-distributed microbial enzyme activities at intact, coated macropore surfaces in Luvisol Bt-horizons. Soil Biol. Biochem. 156, 108193.
Leue, M., Wohld, A., Gerke, H.H., 2018. Two-dimensional distribution of soil organic carbon at intact macropore surfaces in BT-horizons. Soil Tillage Res. 176, 1–9.
Li, H., Van den Bulcke, J., Kibleur, P., Mendoza, O., De Neve, S., Sleutel, S., 2022. Soil textural control on moisture distribution at the microscale and its effect on added particulate organic matter mineralization. Soil Biol. Biochem. 172, 108777.
Liang, A., Zhang, Y., Zhang, X., Yang, X., McLaughlin, N., Chen, X., Guo, Y., Jia, S., Zhang, S., Wang, L., Tang, J., 2021. Investigations of relationships among aggregate pore structure, microbial biomass, and soil organic carbon in a Mollisol using combined nondestructive measurements and phospholipid fatty acid analysis. Soil Tillage Res. 185, 94–101.
Linkosalo, T., Kolari, P., Pumpanen, J., 2013. New decomposition rate functions based on volumetric soil water content for the ROMUL soil organic matter dynamics model. Ecol. Model. 263, 109–118.
Lipiec, J., Kuś, J., Słowińska-Jurkiewicz, A., Nosalewicz, A., 2006. Soil porosity and water infiltration as influenced by tillage methods. Soil Tillage Res. 89 (2), 210–220.
Lucas, M., Nguyen, L., Guber, A., Kravchenko, A., 2022. Cover crop influence on pore size distribution and biopore dynamics: enumerating root and soil faunal effects. Front. Plant Sci. 13. https://doi.org/10.3389/fpls.2022.928569.
Lucas, M., Rohe, L., Apelt, B., Stange, C.F., Vogel, H.-J., Well, R., Schlüter, S., 2024. The distribution of particulate organic matter in the heterogeneous soil matrix - balancing between aerobic respiration and denitrification. Sci. Total Environ. 951. https://doi.org/10.1016/j.scitotenv.2024.175383.
Meurer, K., Chenu, C., Coucheney, E., Herrmann, A., Keller, T., Kätterer, T., Nimblad Svensson, D., Jarvis, N., 2020. Modelling dynamic interactions between soil structure and the storage and turnover of soil organic matter. Biogeosciences 17, 5025–5042.
Moyano, F.E., Vasilyeva, N., Bouckaert, L., Cook, F., Craine, J., Curiel Yuste, J., Don, A., Epron, D., Formanek, P., Franzluebbers, A., Ilstedt, U., Kätterer, T., Orchard, V., Reichstein, M., Rey, A., Ruamps, L., Subke, J.A., Thomsen, I.K., Chenu, C., 2012. The moisture response of soil heterotrophic respiration: Interaction with soil properties. Biogeosciences 9 (3), 1173–1182.
Nimblad Svensson, D., Messing, I., Barron, J., 2022. An investigation in laser diffraction soil particle size distribution analysis to obtain compatible results with sieve and pipette method. Soil Tillage Res. 223, 105450.
Nunan, N., Wu, K., Young, I.M., Crawford, J.W., Ritz, K., 2003. Spatial distribution of bacterial communities and their relationships with the micro-architecture of soil. FEMS Microbiol. Ecol. 44 (2), 203–215.
Pallandt, M., Ahrens, B., Koirala, S., Lange, H., Reichstein, M., Schrumpf, M., Zaehle, S., 2022. Vertically divergent responses of SOC decomposition to soil moisture in a changing climate. J. Geophys. Res.: Biogeosci. 127 (2), 1–16.
Pankhurst, C., et al., 2002. Microbiological and chemical properties of soil associated with macropores at different depths in a red-duplex soil in NSW Australia. Plant Soil 238, 11–20.
Patel, K.F., Myers-Pigg, A., Bond-Lamberty, B., Fansler, S.J., Norris, C.G., McKever, S.A., Zheng, J., Rod, K.A., Bailey, V.L., 2021. Soil carbon dynamics during drying vs. rewetting: importance of antecedent moisture conditions. Soil Biol. Biochem. 156, 108165.
Peth, S., Chenu, C., Leblond, N., Mordhorst, A., Garnier, P., Nunan, N., Pot, V., Ogurreck, M., Beckmann, F., 2014. Localization of soil organic matter in soil aggregates using synchrotron-based X-ray microtomography. Soil Biol. Biochem. 78, 189–194.
Quigley, M., Negassa, W., Guber, A., Rivers, M., Kravchenko, A., 2018. Influence of pore characteristics on the fate and distribution of newly added carbon. Front. Environ. Sci. 6, 51.
R Core Team (2023). R: A Language and Environment for Statistical. Computing_. R Foundation for Statistical Computing, Vienna, Austria. (⟨https://www.R-project.org/⟩).
Rawlins, B.G., Wragg, J., Reinhard, C., Atwood, R.C., Houston, A., Lark, R.M., Rudolph, S., 2016. Three-dimensional soil organic matter distribution, accessibility and microbial respiration in macroaggregates using osmium staining and synchrotron X-ray computed tomography. Soil 2 (4), 659–671.
Reeves, D.W., 1997. The role of soil organic matter in maintaining soil quality in continuous cropping systems. Soil Tillage Res. 43 (1–2), 131–167.
Renard, P., Allard, D., 2013. Connectivity metrics for subsurface flow and transport. Adv. Water Resour. 51, 168–196.
Rey, A., Petsikos, C., Jarvis, P.G., Grace, J., 2005. Effect of temperature and moisture on rates of carbon mineralization in a Mediterranean oak forest soil under controlled and field conditions. Eur. J. Soil Sci. 56 (5), 589–599.
Rumpel, C., Kögel-Knabner, I., 2011. Deep soil organic matter-a key but poorly understood component of terrestrial C cycle. Plant Soil 338 (1), 143–158.
Salome, C., Nunan, N., Pouteau, V., Lerch, T.Z., Chenu, C., 2010. Carbon dynamics in topsoil and in subsoil may be controlled by different regulatory mechanisms. Glob. Change Biol. 16, 416–426.
Schindelin, J., Arganda-Carreras, I., Frise, E., Kaynig, V., Longair, M., Pietzsch, T., Preibisch, S., Rueden, C., Saalfeld, S., Schmid, B., Tinevez, J.Y., White, D.J., Hartenstein, V., Eliceiri, K., Tomancak, P., Cardona, A., 2012. Fiji: An open-source platform for biological-image analysis. Nat. Methods 9 (7), 676–682.
Schlüter, S., Leuther, F., Albrecht, L., Hoeschen, C., Kilian, R., Surey, R., Mikutta, R., Kaiser, K., Mueller, C.W., Vogel, H.J., 2022. Microscale carbon distribution around pores and particulate organic matter varies with soil moisture regime. Nat. Commun. 13 (1).
Schlüter, S., Lucas, M., Grosz, B., Ippisch, O., Zawallich, J., He, H., Dechow, R., Kraus, D., Blagodatsky, S., Senbayram, M., Kravchenko, A., Vogel, H.-J., Well, R., 2024. The anaerobic soil volume as a controlling factor of denitrification: a review. Biol. Fertil. Soils. https://doi.org/10.1007/s00374-024-01819-8.
Schlüter, S., Sheppard, A., Brown, K., Wildenschild, D., 2014. Image processing of multiphase images obtained via X-ray microtomography: a review. Water Resour. Res. 50, 3615–3639.
Schmidt, H., Vetterlein, D., Köhne, J.M., Eickhorst, T., 2015. Negligible effect of X-ray μ-CT scanning on archaea and bacteria in an agricultural soil. Soil Biol. Biochem. 84, 21–27.
Shamonin, D.P., Bron, E.E., Lelieveldt, B.P., Smits, M., Klein, S., Staring, M. & Initiative, A.S.D.N.. (2014). Fast parallel image registration on CPU and GPU for diagnostic classification of Alzheimer's disease. Frontiers in neuroinformatics 7, 50.
Sierra, C.A., Trumbore, S.E., Davidson, E.A., Vicca, S., Janssens, I., 2015. Sensitivity of decomposition rates of soil organic matter with respect to simultaneous changes in temperature and moisture. J. Adv. Model. Earth Syst. 7, 335–356.
Skopp, J., Jawson, M., Doran, J., 1990. Steady-state aerobic microbial activity as a function of soil water content. Soil Sci. Soc. Am. J. 54, 1619–1625.
Smirnova, N., Demyan, M., Rasche, F., Cadisch, G., Müller, T., 2014. Calibration of CO2 trapping in alkaline solutions during soil incubation at varying temperatures using a respicond VI. Open J. Soil Sci. 4, 161–167. https://doi.org/10.4236/ojss.2014.45019.
Stockmann, U., Padarian, J., McBratney, A., Minasny, B., de Brogniez, D., Montanarella, L., Hong, S.Y., Rawlins, B.G., Field, D.J., 2015. Global soil organic carbon assessment. Glob. Food Secur. 6, 9–16.
Strudley, M., Green, T., Ascough II, J., 2008. Tillage effects on soil hydraulic properties in space and time: state of the science. Soil Tillage Res. 99, 4–48.
Sun, B., Chen, X., Zhang, X., Liang, A., Whalen, J., McLaughlin, N., 2020. Greater fungal and bacterial biomass in soil large macropores under no-tillage than mouldboard ploughing. Eur. J. Soil Biol. 97, 103155.
Toosi, E., Kravchenko, A., Guber, A., Rivers, M., 2017. Pore characteristics regulate priming and fate of carbon from plant residue. Soil Biol. Biochem. 113, 219–230.
Vos, C., Don, A., Hobley, E.U., Prietz, R., Heidkamp, A., Freibauer, A., 2019. Factors controlling the variation in organic carbon stocks in agricultural soils of Germany. Eur. J. Soil Sci. 70 (3), 550–564.
Wang, W., Kravchenko, A., Smucker, A., Liang, W., Rivers, M., 2012. Intra-aggregate pore characteristics: X-ray computed microtomography analysis. Soil Sci. Soc. Am. J. 76, 1159–1171.
Wickland, K.P., Neff, J.C., 2008. Decomposition of soil organic matter from boreal black spruce forest: environmental and chemical controls. Biogeochemistry 87 (1), 29–47.
Yin, X., Beaudoin, N., Ferchaud, F., Mary, B., Strullu, L., Chlébowski, F., Clivot, H., Herre, C., Duval, J., Louarn, G., 2020. Long-term modelling of soil N mineralization and N fate using STICS in a 34-year crop rotation experiment. Geoderma 357 (March 2019), 113956.
Yoo, G., Spomer, L., Wander, M., 2006. Regulation of carbon mineralization rates by soil structure and water in an agricultural field and a prairie-like soil. Geoderma 135, 16–25.
Zhang, W., Munkholm, L., Liu, X., An, T., Xu, Y., Ge, Z., Xie, N., Li, A., Dong, Y., Peng, C., Li, S., Wang, J., 2023. Soil aggregate microstructure and microbial community structure mediate soil organic carbon accumulation: evidence from one-year field experiment. Geoderma 430, 116324.
Zheng, J., Bond-Lamberty, B., Bailey, V., 2022. Revisiting diffusion-based moisture functions: why do they fail? Soil Biol. Biochem. 165, 108525.